metals

MDPI

Article

Effect of Quench Polish Quench Nitriding Temperature on the Microstructure and Wear Resistance of SAF2906 Duplex Stainless Steel

Hongliang Xiang [1,2,*], Gaoxiang Wu [1], Dong Liu [1], Huatang Cao [3] and Xuanpu Dong [4]

1 School of Mechanical Engineering and Automation, Fuzhou University, Fuzhou 350116, China
2 Jinjiang Science and Education Park, Fuzhou University, Jinjiang 362251, China
3 Department of Advanced Production Engineering, Engineering and Technology Institute Groningen, University of Groningen, Nijenborgh 4, 9747AG Groningen, The Netherlands
4 State Key Laboratory of Materials Processing and Die & Mould Technology, Huazhong University of Science and Technology, Wuhan 430074, China
* Correspondence: hlxiang@fzu.edu.cn; Tel.: +86-0591-2286-6270

Received: 19 June 2019; Accepted: 30 July 2019; Published: 31 July 2019

Abstract: The effect of quench polish quench (QPQ) nitriding temperature on the microstructure and wear resistance of SAF2906 duplex stainless steel was investigated. Results showed the surface of the nitrided samples was composed of an oxidized layer, a loose compound layer, a compact compound layer, and a diffusion layer. The oxidized layer was composed of Fe_3O_4. The main phases of the loose compound layer were CrN, α_N, $Fe_{2-3}N$, and Fe_3O_4. The compact compound layer was composed of CrN, α_N, and $Fe_{2-3}N$. In the diffusion layer, CrN and expanded austenite (S) were the main phases. The nitrided layer thickness increased from 20 to 41 μm with an increasing temperature of 570 to 610 °C. When the nitriding temperature was above 590 °C, the precipitates in the diffusion layer became coarsened, and their morphologies gradually changed from spherical particulate to rod-like and flocculent-like. Tribotests showed the cumulative mass loss of QPQ-treated samples was much lower than that of the substrate. The cumulative mass loss of the samples nitrided at 610 °C was higher than that at 570 °C during the first 29 h. When the test time was over 29 h, the former was lower than the latter.

Keywords: SAF2906 duplex stainless steel; nitriding temperature; microstructure; wear resistance

1. Introduction

Due to the excellent combination of mechanical properties and corrosion resistance, duplex stainless steel has been widely used in various fields, such as petroleum-refining, chemical, and oceanic industries [1–3]. SAF2906 duplex stainless steel, released by Sweden Sandvik in 2006, was developed on the basis of the third-generation nitrogen-containing duplex stainless steel of 00Cr25Ni7Mo4N. The pitting resistance equivalent number (PREN) of SAF2906 is more than 42, which makes it a hyper duplex stainless steel. In comparison with the third-generation duplex stainless steel, SAF2906 duplex stainless steel possesses higher strength and corrosion resistance, making it an ideal candidate used in marine industries [4]. Moreover, as a substitute for 304 or 316L stainless steels, SAF2906 duplex stainless steel can improve the service life and reduce the weight. However, the low hardness and, in particular, the poor wear resistance limits its wide applications, which highlights the significance to enhance the wear resistance. Quench polish quench (QPQ) is an environmentally friendly heat treatment technology for metal surfaces which contributes to improving mechanical properties and corrosion resistance at low cost and with low part distortion [5,6]. As a comprehensive method of metal surface strengthening, its essence is the combination of nitriding and oxidation processes. The microstructure

obtained in the nitriding layer also consists of both nitrides and oxides. After nitriding and oxidation treatment, a high-hardness and compact infiltration layer will be formed on the surface of the materials, which can significantly improve their wear resistance and thus also prolong the properties comprehensively [7,8]. According to the process temperature, QPQ treatment can be classified into two categories. One treatment is the ferritic nitrocarburizing, which is carried out at temperatures below the eutectic point (590 °C) according to the Fe–N diagram, and the other is austenitic nitrocarburizing, which is carried out above the eutectic point [9]. A considerable number of studies on the effect of ferritic nitrocarburizing on the microstructure and wear resistance of stainless steels have been reported [6,10–13]. It was found that the high wear resistance of stainless steels is mainly attributed to the formation of hard and dispersed nitrides (e.g., CrN and $Fe_{2-3}N$) on the surface after QPQ treatment. However, both the thin layer of the nitrides and the low nitriding temperature (the latter leads to a larger consumption of time and energy) would limit their applications, such as in high-speed or heavy load services. Therefore, it is necessary to increase the surface nitriding layer thickness of stainless steels. Cai and Wang et al. [14,15] reported that when the nitriding temperature increased over 590 °C, austenitic nitrocarburizing occurred, and the surface layer thickness of stainless steels reached twice as thick as that heat-treated below 590 °C. However, there are rare studies on the influence of austenitic nitrocarburizing on stainless steels. At present, the QPQ technology is mainly used on single-phase steels, and even less work has been devoted to the effect of QPQ treatment on SAF2906 duplex stainless steel. In this paper, the microstructure, microhardness and wear resistance of the surface layer of both ferritic nitrocarburizing and austenitic nitrocarburizing were studied, and the effect of QPQ nitriding temperature on the microstructure and wear resistance of SAF2906 duplex stainless steel is discussed.

2. Materials and Methods

SAF2906 duplex stainless steel was prepared by investment casting. The raw material consisted of 316L stainless steel, chromium metal, iron molybdenum, electrolytic nickel, and nitride alloy. They were melted in a 300 kW/30 kg medium frequency induction furnace. Afterwards, the molten steel was poured into a shell mold (Fuzhou Yingtuo Precise Metallurgy Industry Co., Ltd., Fuzhou, China) that was preheated to about 900 °C. The chemical compositions of the as-cast ingot were detected by ARL100 optical emission spectrometry (ARL Corp., Bern, Switzerland), as shown in Table 1. The ingot was solution treated at 1050 °C for 2 h followed by water quenching. Several samples of 10 mm × 10 mm × 10 mm were cut from the ingot for microstructure and hardness examinations. Samples of 30 mm × 7 mm × 6 mm were also cut for wear resistance tests.

Table 1. Chemical compositions of SAF2906 DSS sample (wt %).

C	Si	Mn	P	S	Ni	Cr	Mo	Cu	N	Fe
0.03	0.72	0.81	0.02	0.02	6.61	29.19	2.11	0.79	0.26	Balance

The samples were cleaned with acetone and anhydrous ethanol in an ultrasonic instrument (Keer Ulrasonec Cleaning Equipment Co., Ltd., Jinan, China) to remove oil stains on the surface of the substrate, and the preheating was carried out at 400 °C for 30 min. Then, the samples were separately nitrided at 550, 570, 590, and 610 °C for 150 min, followed by the same post-oxidation process with a heating temperature at 400 °C for 30 min. The cyanate ion concentration in QPQ salt bath pit-type furnace was 33%. Finally, the samples were cleaned for further characterization.

The cross-section microstructure of the QPQ-treated samples was observed by XJP-300 optical microscope (OM) (Olympus Corporation, Tokyo, Japan) and S-3000N scanning electron microscope (SEM) (Hitachi Co., Ltd., Tokyo, Japan) after metallographic preparation and etching in Murakami reagent (10 g potassium hydroxide, 10 g potassium ferricyanide, and 100 mL distilled water). The phase compositions of the surface layers were detected by X'Pert Pro MPD X-ray diffractometry (Royal Dutch Philips Electronics Ltd., Amsterdam, The Netherlands) with Co Kα radiation in the 2θ range from

20° to 100°. Cross-sectional elemental depth profiles of the treated samples were obtained by energy disperse spectroscopy (EDS) (Bruker Nano GmbH, Berlin, Germany). The hardness was measured by MVC-1000D1 microhardness tester (Shanghai Jiming Measuring Equipment Co., Ltd., Shanghai, China) using a load of 200 g for 15 s, taking 10 measurements to determine the average value. According to the GB/T 12444.1 standard, dry sliding tribological tests were carried out on an MMS-2A tribometer (Jinan Yihua Tribology Testing Technology Co., Ltd., Jinan, China) with GCr15 steel counterpart balls (40 mm in diameter) rotated at a speed of 200 rpm and a load of 50 N against the surface of the samples. Before tests, both the non-treated and treated samples were cleaned with alcohol. They were cleaned and dried after a certain time interval, and were then measured using a FA2014 electron analytical balance (Tianjin Tianma Hengji Instrument Co., Ltd., Tianjin, China) with an accuracy of 0.1 mg. The average mass loss was calculated by three parallel experiments carried out under the same conditions.

3. Results and Discussion

3.1. Metallographic Observation

Figure 1 shows the cross-sectional microstructure of the samples of SAF2906 duplex stainless steel nitrided at different temperatures of 550, 570, 590, and 610 °C. It is observed that the cross-sectional microstructure of the samples after ferritic nitrocarburizing and austenitic nitrocarburizing are obviously different. The surface layer of ferritic nitrocarburizing samples consists of an oxide layer, a compact compound layer and a diffusion layer from the outermost surface to the center.

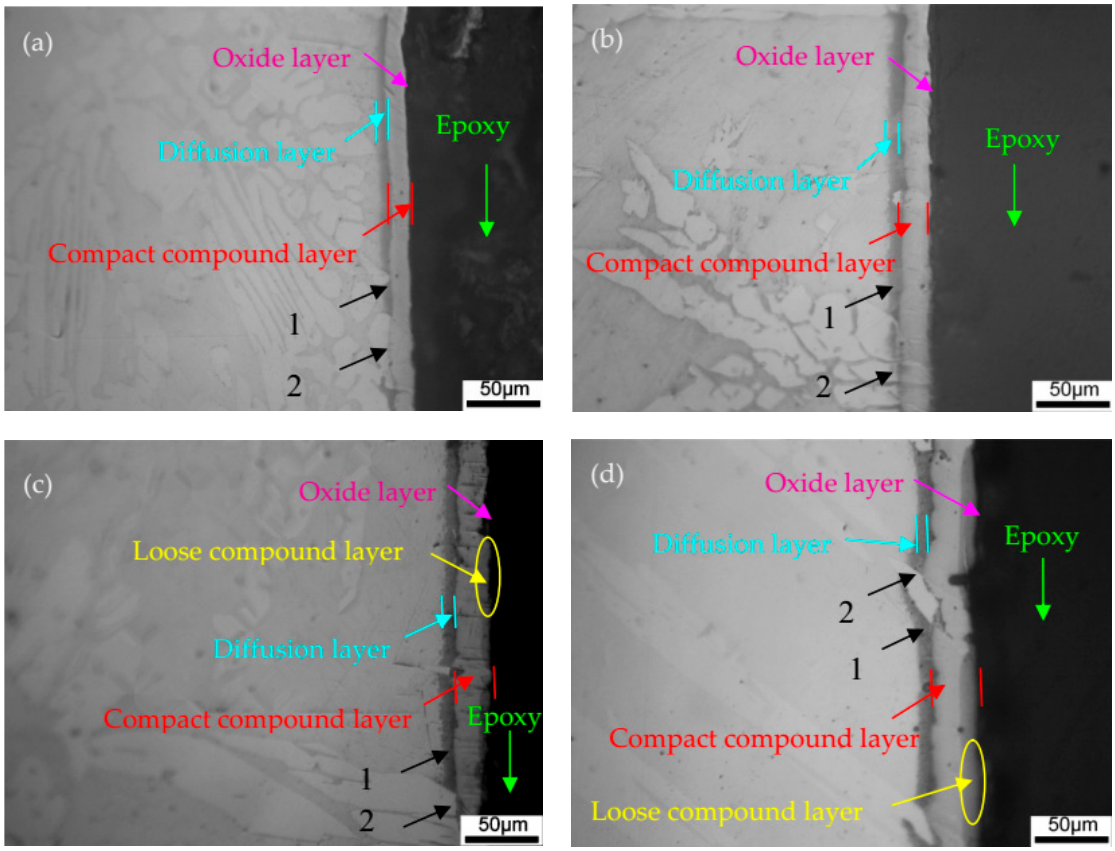

Figure 1. Cross-sectional microstructure of the samples nitrided at different temperatures: (**a**) 550 °C; (**b**) 570 °C; (**c**) 590 °C; (**d**) 610 °C.

However, the surface layer of austenitic nitrocarburizing samples consists of an oxidized layer, a loose compound layer, a compact compound layer and a diffusion layer. The oxidized layer is about 1–2 μm, as indicated by the pink arrows shown in Figure 1. The compound layer is composed of

loose (as indicated by the yellow arrows in Figure 1) and compact (as indicated by the red arrows in Figure 1) compound layers. The diffusion layer (see the region as indicated by the turquoise arrows in Figure 1) is a transition zone between the compound layer and the substrate. Two parts can be observed: one is in the dark region (denoted as region 1) and the other in the bright region (denoted as region 2). The reason for the dark region is that the solubility of nitrogen in ferrite is small, resulting in the diffusion of nitrogen into ferrite. The nitrogen later easily combines with a high concentration of chromium to form chromium nitride (CrN). This subsequently leads to Cr-depleted areas in the matrix and deteriorates its corrosion resistance. After the reagent etching, the region appears dark. The brighter appearance of region 2 is mainly due to the original microstructure where there is austenite, and more nitrogen atoms could be dissolved into austenite during the nitriding process, which increases its corrosion resistance [16,17]. Therefore, the region appears bright after reagent etching. The thicknesses of the nitrided layers are approximately 20, 25, 33, and 41 μm for samples nitrided at 550, 570, 590, and 610 °C, respectively, indicating that the nitrided layer thickness increases as the temperature increases. In addition, it can be seen that there is some loose microstructure appearing in the compound layer in the samples nitrided at 590 and 610 °C. The higher the temperature, the wider the loose microstructure.

To further study the effect of the nitriding temperature on the microstructure, typical samples of ferritic nitrocarburizing (570 °C, see Figure 1b) and austenitic nitrocarburizing (610 °C, see Figure 1d) were scrutinized for high-magnification SEM observations, as shown in Figure 2.

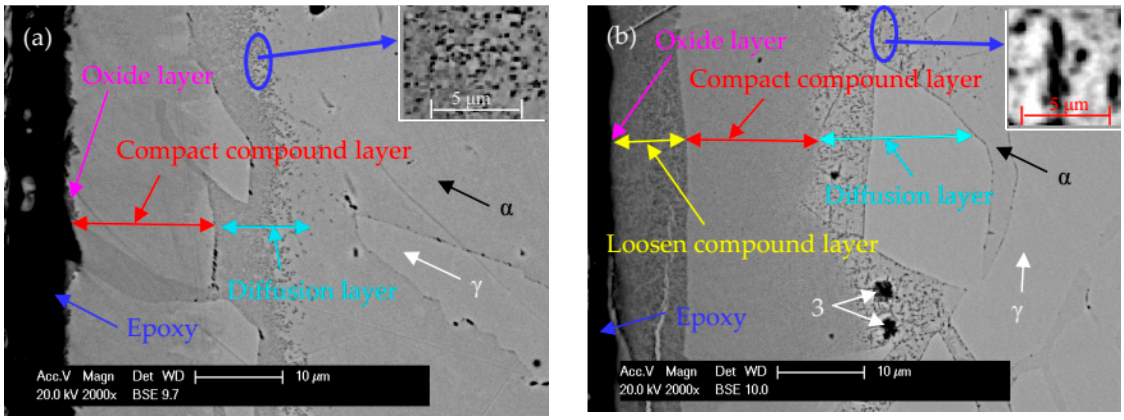

Figure 2. Cross-sectional SEM images of microstructure of the samples nitrided at two temperatures: (**a**) 570 °C; (**b**) 610 °C.

As can be seen, both the nitrided layer thickness and the compound layer morphology change, and the precipitates exhibit different morphologies. In the sample heat-treated at 570 °C, the CrN precipitates appear to be spherical and granular, while for that treated at 610 °C, they are spherical granular as well as rod-like and flocculent-like, as indicated by the inset and arrow 3 marked in Figure 2b. It is thus clear that this morphology difference is attributed to the different high nitriding temperature.

3.2. XRD Analysis

Microstructure observation shows that the morphology of the nitrided layer changes when the nitriding temperature is higher than 590 °C. To evaluate the effect of the nitriding temperature on the phase compositions of the surface layer, the substrate and typical samples of ferritic nitrocarburizing (Figure 1b) and austenitic nitrocarburizing (Figure 1d) were selected for XRD tests. The results are shown in Figure 3.

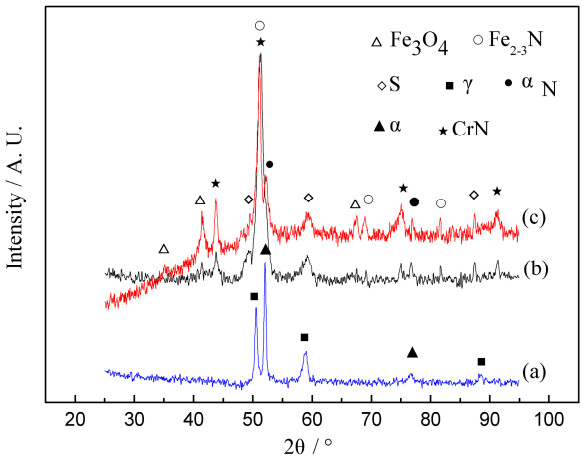

Figure 3. X-ray diffraction patterns of the substrate (**a**) and two specimens: (**b**) 570 °C; (**c**) 610 °C.

It can be seen that the surface layer of these two typical samples consists of CrN, α_N (expanded martensite), Fe_3O_4, $Fe_{2–3}N$, and S (expanded austenite). In addition, the diffraction peaks of α and γ from the substrate are no longer observed because X-ray is unable to penetrate from the thick surface layer to the substrate. Compared with the 2 θ of α and γ, the diffraction peaks of α_N and S are shifted towards low angles, indicating that nitrogen supersaturated in crystals causes the lattice expansion and some increase in the lattice constant. This results in the formation of α_N and S with the same structure of α and γ, respectively [18–20]. It is generally believed that the carbides act as the nuclei of $Fe_{2–3}N$ crystal. When the content of solution nitrogen reaches a certain degree, the $Fe_{2–3}N$ crystal could form [21]. It is also found that the α_N and CrN diffraction peak intensities of the sample treated at 610 °C are higher than that at 570 °C. This indicates that there are more α_N and CrN in the former because the higher temperature facilitates nitrogen activities, leading to more nitrogen dissolved into S phase. Ultimately, it also increases its lattice distortion and residual stress and leads to more transformation of S phase to α_N and CrN.

3.3. EDS Analysis

Figure 4 displays the EDS line scans of oxygen, nitrogen, iron, and chromium of the typical samples of ferritic nitrocarburizing (Figure 2a) and austenitic nitrocarburizing (Figure 2b), from the surface to the center (0–90 μm). From Figure 4a,b, it can be seen that the thickness of the oxidized layer (characteristic of a high oxygen concentration) of the sample treated at 570 °C is about 3 μm, while it increases to approximately 10 μm at 610 °C. The reason is that the loose compound layer at 610 °C is thicker than that at 570 °C. It is a sponge-like or columnar porous structure that makes oxygen atoms to diffuse easily into the inner layer through these micropores, promoting the formation of Fe_3O_4. In contrast, the oxygen concentration in other layers closer to the substrate is rather low. This implies that the existence of micropores promotes the oxygen diffusion.

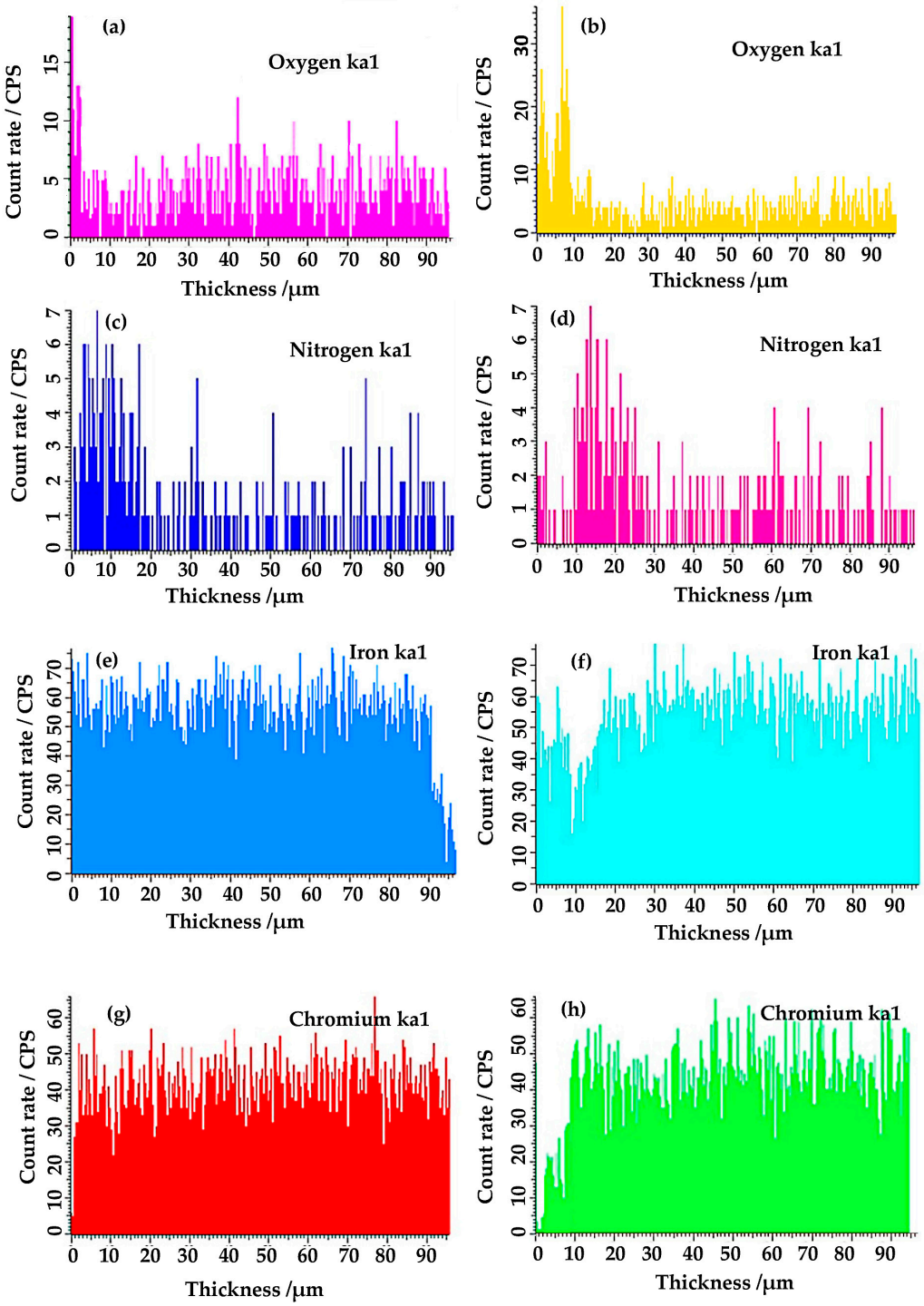

Figure 4. EDS analysis results (from surface to the center): (**a**,**c**,**e**,**g**) of 570 °C nitriding sample; (**b**,**d**,**f**,**h**) of 610 °C nitriding sample.

For nitrogen, it can be seen from Figure 4c,d that the nitrogen concentrations of the compact compound layer both at 570 and 610 °C are significantly higher than those of the substrate. However, the nitrogen concentration of the loose compound layer at 610 °C is close to the substrate. Schröter [22] considered the less nitrogen in the loose compound layer as a result of the recombination and escape of molecular nitrogen. In Figure 4c,d, peaks of nitrogen concentration in the nitrocarburizing layer were found at layers with the thickness of about 7 and 15 μm at 570 and 610 °C, respectively. Some studies [23,24] also reported the same phenomenon. Owing to the oxidation reaction at the

surface after nitriding treatment, the diffusion of iron atoms from the nitride layer to the surface occurs to form Fe_3O_4 and renders the nitrogen atoms redistributed underneath the oxide layer. The reason for the larger thickness of the nitrogen concentration at 610 °C might be associated with more paths for oxygen atoms to diffuse into the compound layer. On the contrary, the loose microstructure in the sample treated at 610 °C aids oxygen atoms to diffuse into the inner of the compound layer and promotes the scope of oxidation reaction, which makes the nitrogen accumulation position backward.

As shown in Figure 4e,f, the iron concentration of the compact compound layer at 570 and 610 °C are both lower than that of the substrate. However, in the loose compound layer at 610 °C, it is close to the substrate. This indicates that the loose compound layer is rich in iron. The chromium concentration profiles of the two samples are presented in Figure 4g,h. Apart from the oxide layer, the surface layer at 570 °C is rich in chromium, and the chromium concentration in the loose compound layer at 610 °C is much less than that in the compact compound layer.

From the analysis above, it can be concluded that the loose compound layer is rich in iron and oxygen, but deficient in chromium and nitrogen. For the compact compound layer, however, it is opposite. This is consistent with the results analyzed above that the color of the loose compound layer microstructure after etching is darker than the compact one, which verifies the difference in the compositions.

Based on the cross-sectional microstructure analysis and the results by EDS and XRD, it can be concluded that the oxide layer is composed of Fe_3O_4; the main phases of the loose compound layer are CrN, α_N, $Fe_{2-3}N$, and Fe_3O_4, among which Fe_3O_4 and $Fe_{2-3}N$ are dominant; the compact compound layer is mainly composed of CrN, α_N, and $Fe_{2-3}N$, and the amount of CrN is higher than that of the other two. However, in the diffusion layer, CrN and S are the main phases.

3.4. Hardness Analysis

The substrate and four samples treated at 550, 570, 590, and 610 °C were selected for microhardness tests, and the results are shown in Figure 5.

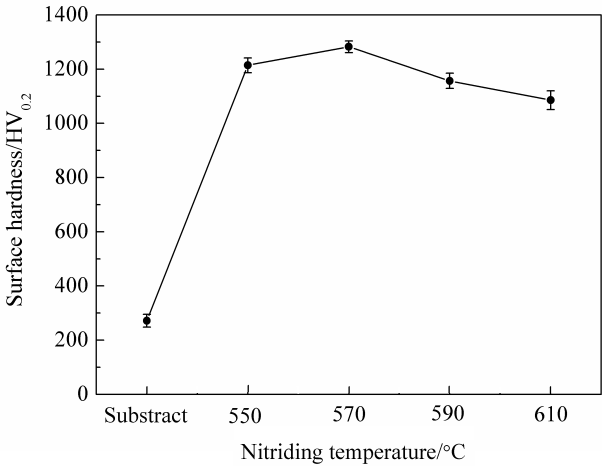

Figure 5. Surface hardness of the substrate and two samples.

The surface hardness of the samples after QPQ treatment is triple that of the substrate. This dramatic increase in the hardness is due to the modifications of the surface microstructure of the sample after QPQ treatment. The phase developed from soft phases α and γ into hard phases CrN, $Fe_{2-3}N$, and α_N. It is observed that the hardness of the surface of the samples treated at 590 °C (1157 $HV_{0.2}$) and 610 °C (1085 $HV_{0.2}$) is lower than that at 550 °C (1214 $HV_{0.2}$) and 570 °C (1283 $HV_{0.2}$). The explanation for this phenomenon is as follows. Compared with the samples treated at 550 and 570 °C, the outside surface layer at 590 and 610 °C has more low-hardness phases of $Fe_{2-3}N$ and Fe_3O_4, while the amount of the high-hardness CrN is less. When the nitriding temperature reaches temperatures over 590 °C,

the distinct loose microstructure appears in the compound layer, which leads to a lower hardness. Moreover, at higher temperature, the grain of the compound layer and diffusion layer grows and coarsens, which leads to the decrease of surface hardness as well [25].

3.5. Wear Resistance Analysis

To study the influence of QPQ nitriding temperature on wear resistance of SAF2906 duplex stainless steel, the same samples as above were selected for dry sliding tribological test. Since the surface layer structure is complicated, the wear resistance of QPQ nitrocarburizing samples may be different in diverse periods of the tests, and it is difficult to comprehensively reflect its wear resistance during a short test time. Therefore, the total test time was set as 38 h. Due to the loose compound layer with low hardness and poor wear resistance, the time interval for test at the early stage was selected to be 1 h. When the loose compound layer was worn off, the time interval for the test was 3 h. The mass loss curves describing the wear resistance of the QPQ-treated samples are shown in Figure 6. It can be seen that the cumulative mass loss in substrate increases linearly as the test time increases, with a relatively stable wear rate of about 15 mg/h. The cumulative mass loss of the samples treated at 570 °C increases slowly until 23 h, and the wear rate is only 0.65 mg/h. When the test time exceeds 23 h, the wear rate and cumulative mass loss increase significantly. In the sample treated at 610 °C, the cumulative mass loss increases gently before 29 h. The wear rate is 1.3 mg/h for the first 8 h and then drops to 0.75 mg/h until 29 h. When the test time is longer than 29 h, the wear rate and cumulative mass loss increase significantly. Throughout the test, the cumulative mass loss of the QPQ-treated samples is much lower than that of the substrate. Obviously, this phenomenon is related to the surface microstructural change of the samples. When the surface microstructure consists of hard phases (CrN, $Fe_{2–3}N$, or α_N), the samples showed a good wear resistance. By contrast, when the sample is composed of soft phases (α and γ), the wear resistance is low. Moreover, the cumulative mass loss of the two samples show an intersection at 29 h, before which the cumulative mass loss of sample nitrided at 570 °C is lower than that at 610 °C, but the opposite trend starts after 29 h. This phenomenon is owed to the distinct loose microstructures in the surface layer of the samples nitrided at 610 °C, and this results in lower hardness value, as the curves with a testing time less than 29 h shown in Figure 6.

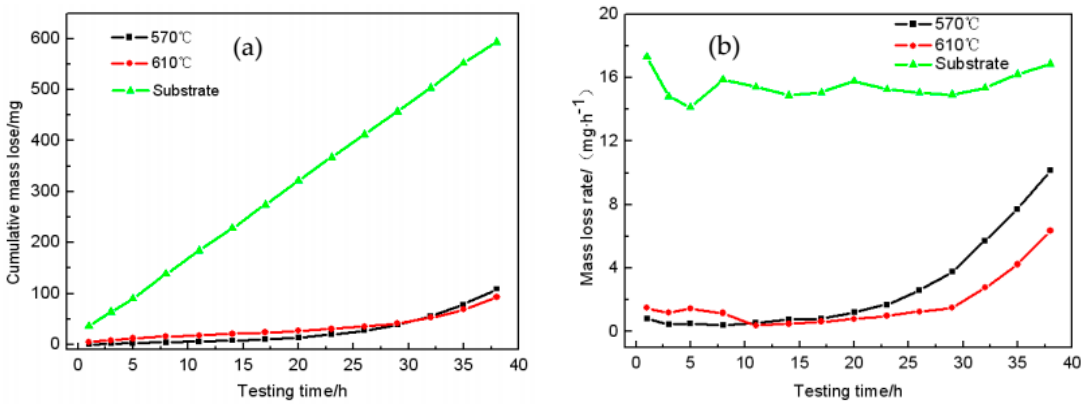

Figure 6. Mass loss and rate curves of the substrate and two samples: (**a**) cumulative mass loss curve; (**b**) mass loss rate curve.

With the increase of testing time, the loose compound layer at 610 °C is gradually worn off, and the compact compound layer with higher hardness is exposed and starts to play a role. Consequently, the wear rate decreases. When the testing time is over 11 h, the wear rate of the sample nitrided at 610 °C is lower than that at 570 °C. In the case of over 29 h, the cumulative mass loss of the former is higher than the latter.

4. Conclusions

This study aims to obtain an underlying understanding of the effect of QPQ nitriding temperature on the microstructure and wear resistance of SAF2906 duplex stainless steel. The results are summarized as follows:

1. The surface layer of the samples after ferritic nitrocarburizing was composed of an oxidized layer, a compact compound layer, and a diffusion layer from the outmost surface to the center. The surface layer after austenitic nitrocarburizing was composed of an oxidized layer, a loose compound layer, a compact compound layer, and a diffusion layer. The oxidized layer was primarily composed of Fe_3O_4. The main phase of the loose compound layer was CrN, α_N, $Fe_{2-3}N$, and Fe_3O_4, among which $Fe_{2-3}N$ and Fe_3O_4 were dominant. The compact compound layer mainly consisted of CrN, together with certain α_N and $Fe_{2-3}N$. However, in the diffusion layer, CrN and S were the main phases.
2. With the increasing temperature, the thickness of the nitrided layer increased dramatically from 20 μm at 550 °C to 41 μm at 610 °C. When the temperature was above 590 °C, the precipitates of the diffusion layer became coarsened, and their morphologies gradually changed from spherical particle into rod-like and flocculent-like ones. The surface hardness of the QPQ-treated samples was more than 1090 $HV_{0.2}$ and 3 times that of the substrate.
3. The cumulative mass loss of QPQ-treated samples was much lower than that of the substrate. The cumulative mass loss of samples nitrided at 610 °C was higher than that at 570 °C during the first 29 h. When the test time was over 29 h, the former was lower than the latter. Overall, the wear resistance of samples nitrided at 610 °C was higher than that at 570 °C.
4. In general, the sample nitrided at 610 °C with a deeper surface reinforced layer has better wear resistance than that at 570 °C. The wear resistance of QPQ-treated samples depends not only on the surface hardness, but also largely on the thickness and microstructure of the modified surface layer.

Author Contributions: Conceptualization, H.X.; methodology, G.W.; validation, H.X., G.W., and D.L.; formal analysis, H.X.; investigation, H.X.; resources, G.W.; data curation, G.W.; writing—original draft preparation, H.X.; writing—review and editing, H.X., H.C. and X.D.; visualization, H.X.; supervision, H.X.; project administration, H.X.; funding acquisition, H.X.

Funding: This research was funded by the National Natural Science Foundation of China (grant number 51601039), Major Special Projects of Science and Technology of Fujian Province (grant number 2017HZ0001-2), Industrial Technology Joint-Innovation Projects of Fujian Province (grant number FG-2016001), and Program for New Century Excellent Talents in University of Fujian Province (grant number JA10014).

Conflicts of Interest: The authors declare no conflict of interest.

References

1. Zanotto, F.; Grassi, V.; Balbo, A.; Zucchi, F.; Monticelli, C. Investigation on the corrosion behavior of lean duplex stainless steel 2404 after aging within the 650–850 °C temperature range. *Metals* **2019**, *9*, 529. [CrossRef]
2. Argandoña, G.; Palacio, J.; Berlanga, C.; Biezma, M.; Rivero, P.; Peña, J.; Rodriguez, R. Effect of the temperature in the mechanical properties of austenite, ferrite and sigma phases of duplex stainless steels using hardness. *Metals* **2017**, *7*, 219. [CrossRef]
3. Campos, M.; Bautista, A.; Caceres, D.; Abenojar, J.; Torralba, J.M. Study of the interfaces between austenite and ferrite grains in P/M duplex stainless steels. *J. Eur. Ceram. Soc.* **2003**, *23*, 2813–2819. [CrossRef]
4. Tan, H.; Jiang, Y.M.; Deng, B.; Sun, T.; Xu, J.; Li, J. Effect of annealing temperature on the pitting corrosion resistance of super duplex stainless steel UNS S32750. *Mater. Charact.* **2009**, *60*, 1049–1054. [CrossRef]
5. Yeung, C.F.; Lau, K.H.; Li, H.Y.; Luo, D.F. Advanced QPQ complex salt bath heat treatment. *J. Mater. Process. Technol.* **1997**, *66*, 249–252. [CrossRef]

6. Li, G.L.; Peng, Q.; Wang, J.; Li, C.; Wang, Y.; Gao, J.; Chen, S.Y.; Shen, B.L. Surface microstructure of 316L austenitic stainless steel by the salt bath nitrocar burizing and post-oxidation process known as QPQ. *Surf. Coat. Technol.* **2008**, *202*, 2865–2870. [CrossRef]
7. Zhang, L.; Ren, C.; Yu, Q.; Zhang, J.; Sun, S.Q.; Ren, Q.S.; Lian, Y.; Chen, X.L.; Gao, W. Microstructure and properties of 1Cr12Ni2WMoVNb (GX-8) steel bored barrels with and without QPQ treatment. *Surf. Coat. Technol.* **2017**, *315*, 95–104. [CrossRef]
8. Pokorný, Z.; Kadlec, J.; Hrubý, V.; Joska, Z.; Tran, D.Q.; Beran, D. Plasma nitriding of bored barrels. *AiMT* **2011**, *6*, 69–75.
9. Celik, A.; Karakan, M.; Alsaran, A.; Efeoglu, I. The investigation of structural, mechanical and tribological properties of plasma nitrocarburized AISI 1020 steel. *Surf. Coat. Technol.* **2005**, *200*, 1926–1932. [CrossRef]
10. Cai, W.; Meng, F.N.; Gao, X.Y.; Hu, J. Effect of QPQ nitriding time on wear and corrosion behavior of 45 carbon steel. *Appl. Surf. Sci.* **2012**, *261*, 411–414. [CrossRef]
11. Wang, J.; Lin, Y.H.; Fan, H.Y.; Zeng, D.; Peng, Q.; Shen, B. Effects of Temperature on Microstructure and Wear of Salt Bath Nitrided 17-4PH Stainless Steel. *J. Mater. Eng. Perform.* **2012**, *21*, 1708–1713. [CrossRef]
12. Li, G.J.; Peng, Q.; Li, C.; Wang, Y.; Gao, J.; Chen, S.; Wang, J.; Shen, B. Microstructure analysis of 304L austenitic stainless steel by QPQ complex salt bath treatment. *Mater. Charact.* **2008**, *59*, 1359–1363. [CrossRef]
13. Li, G.J.; Wang, J.; Peng, Q.; Li, C.; Wang, Y.; Shen, B. Influence of salt bath nitrocarburizing and post-oxidation process on surface microstructure evolution of 17-4PH stainless steel. *J. Mater. Proc. Technol.* **2008**, *207*, 187–192. [CrossRef]
14. Cai, W.W.; Luo, D.F. Effect of depth QPQ process on microstructure of 3Cr13 steel. *Mater. Heat Treat.* **2012**, *41*, 176–179.
15. Wang, J.; Xiong, J.; Peng, Q. Study on compound nitriding process of 17-4PH stainless steel in salt bath. *Nuclear Power Eng.* **2009**, *30*, 66–71.
16. Loable, C.; Viçosa, I.N.; Mesquita, T.J.; Mantel, M.; Nogueira, R.P.; Berthomé, G.; Chauveau, E.; Roche, V. Synergy between molybdenum and nitrogen on the pitting corrosion and passive film resistance of austenitic stainless steels as a pH-dependent effect. *Mater. Chem. Phys.* **2017**, *186*, 237–245. [CrossRef]
17. Simmons, J.W. Overview: high-nitrogen alloying of stainless steels. *Mater. Sci. Eng. A* **1996**, *207*, 159–169. [CrossRef]
18. Samandi, M.; Shedden, B.A.; Smith, D.I.; Collins, G.A.; Hutchings, R.; Tendys, J. Microstructure, corrosion and tribological behavior of plasma immersion ion-implanted austenitic stainless steel. *Surf. Coat. Technol.* **1993**, *59*, 261–266. [CrossRef]
19. Collins, G.A.; Hutchings, R.; Short, K.T.; Tendys, J.; Li, X.; Samandi, M. Nitriding of austenitic stainless steel by plasma immersion ion implantation. *Surf. Coat. Technol.* **1995**, *74*, 417–424. [CrossRef]
20. Kim, S.K.; Yoo, J.S.; Preiest, J.M.; Fewell, M.P. Characteristics of martensitic stainless steel nitrided in a low-pressure RF plasma. *Surf. Coat. Technol.* **2003**, *163*, 380–385. [CrossRef]
21. Li, H.Y.; Luo, D.F.; Wu, S.X. *The Principle and Application of QPQ Technology*, 1st ed.; China Machine Press: Beijing, China, 2008; pp. 25–47.
22. Schröter, W.; Spengler, A. Contribution to the state of knowledge of pore formation during layer formation by nitrogen in iron materials. Published in the Conference Volume: "Nitrieren", Proceedings of the ATTT/AWT Conference. Aachen, Germany, 10–12 April 2002.
23. Graat, P.C.J.; Somers, M.A.J.; Jmittemeijer, E. The initial oxidation of e-Fe2N1-x: An XPS investigation. *Appl. Surf. Sci.* **1998**, *136*, 238–259. [CrossRef]
24. Jacquet, P.; Coudert, J.B.; Lourdin, P. How different steel grades react to a salt bath nitrocarburizing and post-oxidation process: Influence of alloying elements. *Surf. Coat. Technol.* **2011**, *205*, 4064–4067. [CrossRef]
25. Zhao, L.F.; Wang, X.X. Microstructure and properties of plasma nitrided 00Cr12Ni9Mo4Cu2Ti maraging stainless steel. *Trans. Mater. Heat Treat.* **2009**, *30*, 172–177.